Angus Academic Press AIIETES 2026
ISSN: 3007-9640 DOI: https://doi.org/10.70114/acmsr.2026.9.1.P172

Effect of Nb Content on the Microstructure and Corrosion Behavior of $FeCrNiMoNb_x$ High-Entropy Alloy Coatings for ATF Cladding

Ruida Jiang [1, a], Rui Lan [1, b] *

[1] School of Material Science and Engineering, Jiangsu University of Science and Technology, No.666, Changhui Road, Zhenjiang, Jiangsu Province, 212000, China.

[a] 231110601212@stu.just.edu.cn, [b] dutrlan@just.edu.cn

Abstract. $FeCrNiMoNb_x$ high-entropy alloy coatings with different Nb contents were prepared on Zr alloy substrates by dual-target magnetron co-sputtering for accident tolerant fuel cladding applications. The effects of Nb content on the microstructure, wettability, electrochemical corrosion behavior, and high-temperature and high-pressure water corrosion behavior were investigated. The results showed that all coatings were continuous and mainly exhibited amorphous or low-crystallinity structures. With increasing Nb target power, the Nb content in the coatings gradually increased. Among the investigated coatings, FeCrNiMoNb1.2 exhibited the smoothest and densest surface and the largest water contact angle of 89.4°. In 3.5 wt.% NaCl solution, FeCrNiMoNb1.2 and FeCrNiMoNb1.4 showed lower corrosion current densities than the Zr substrate, indicating improved corrosion resistance. After corrosion in high-temperature and high-pressure water at 360 °C and 18.6 MPa for 72 h, FeCrNiMoNb1.2 showed the smallest mass loss of −5.69 mg/dm2 and retained better surface integrity. The improved performance was mainly attributed to the dense coating structure and the formation of protective Cr2O3 and Nb2O5. Overall, FeCrNiMoNb1.2 exhibited the best comprehensive protective performance and is a promising candidate coating for ATF cladding applications.

Keywords: high-entropy alloy coating; $FeCrNiMoNb_x$; accident tolerant fuel; corrosion resistance

1. Introduction

Zirconium alloys are widely used as nuclear fuel cladding materials in light water reactors because of their low thermal neutron absorption cross-section, good mechanical properties, and mature engineering application[1-3]. However, under severe accident conditions, zirconium alloys suffer from rapid oxidation in high-temperature steam, accompanied by hydrogen release and heat generation[4, 5]. Therefore, protective coatings with improved oxidation and corrosion resistance are considered an effective strategy for enhancing the safety margin of accident tolerant fuel (ATF) claddings.

High-entropy alloy (HEA) coatings have attracted attention for ATF cladding applications due to their compositional designability, multi-element synergy, and high structural stability[6, 7]. In Fe–Cr–Ni–Mo-based coatings, Cr can promote the formation of protective Cr_2O_3[8, 9], Ni contributes to corrosion resistance and structural stability[10, 11], and Mo improves high-temperature stability[12]. Nb, as a refractory element, may further improve the protective ability by promoting the formation of stable Nb_2O_5[13, 14]. However, the effect of Nb content on the structure and corrosion behavior of $FeCrNiMoNb_x$ HEA coatings still needs clarification.

In this work, $FeCrNiMoNb_x$ HEA coatings with different Nb contents were prepared on Zr substrates by dual-target magnetron co-sputtering. The effects of Nb content on the microstructure, wettability, corrosion behavior in 3.5 wt.% NaCl solution, and corrosion behavior in high-temperature and high-pressure water were investigated.

2. Experimental Procedures

$FeCrNiMoNb_x$ HEA coatings were deposited on Zr alloy substrates by dual-target direct-current magnetron co-sputtering using a FeCrNiMo alloy target and a Nb target. Before deposition, the Zr substrates were ground, polished, ultrasonically cleaned, and dried. The base pressure was 5×10^{-5}

ISSN: 3007-9640 DOI: https://doi.org/10.70114/acmsr.2026.9.1.P172
Pa, and high-purity Ar was introduced at 20 sccm. The FeCrNiMo target power was fixed at 150 W, while the Nb target power was set to 15, 25, 50, and 75 W. The deposition time was 6 h. According to the measured Nb contents, the coatings were denoted as $FeCrNiMoNb_{0.3}$, $FeCrNiMoNb_{0.5}$, $FeCrNiMoNb_{1.2}$, and $FeCrNiMoNb_{1.4}$.

The surface morphology and elemental composition were characterized by SEM and EDS. The phase structure was analyzed by XRD using Cu Kα radiation. Surface wettability was evaluated by static water contact angle measurements. Electrochemical corrosion tests were performed in 3.5 wt.% NaCl solution using a three-electrode system. High-temperature and high-pressure water corrosion tests were conducted in static pure water at 360 °C and 18.6 MPa for 72 h.

3. Results and Discussion

3.1 Microstructure of the $FeCrNiMoNb_x$ coatings

$FeCrNiMoNb_x$ HEA coatings with different Nb contents were successfully deposited on Zr alloy substrates. As shown in Table 1, with increasing Nb target power from 15 to 75 W, the Nb content in the coatings increased from 8.70 at.% to 25.45 at.%, indicating that the coating composition could be effectively controlled by co-sputtering. The surface SEM morphologies are shown in Fig. 1. All coatings were continuous without obvious through-thickness cracks or large pores. Among them, the $FeCrNiMoNb_{1.2}$ coating exhibited a smoother and denser surface.

As shown in Fig. 2, no obvious crystalline diffraction peaks from the coatings were observed, except for the peaks of the Zr substrate, indicating that the $FeCrNiMoNb_x$ coatings mainly exhibited amorphous or low-crystallinity structures. The water contact angle results are shown in Fig. 3. The contact angles of $FeCrNiMoNb_{0.3}$, $FeCrNiMoNb_{0.5}$, $FeCrNiMoNb_{1.2}$, and $FeCrNiMoNb_{1.4}$ were 74.2°, 84.1°, 89.4°, and 83.5°, respectively. The largest contact angle of $FeCrNiMoNb_{1.2}$ suggests its relatively low surface wettability, which may help reduce the contact between corrosive media and the coating surface.

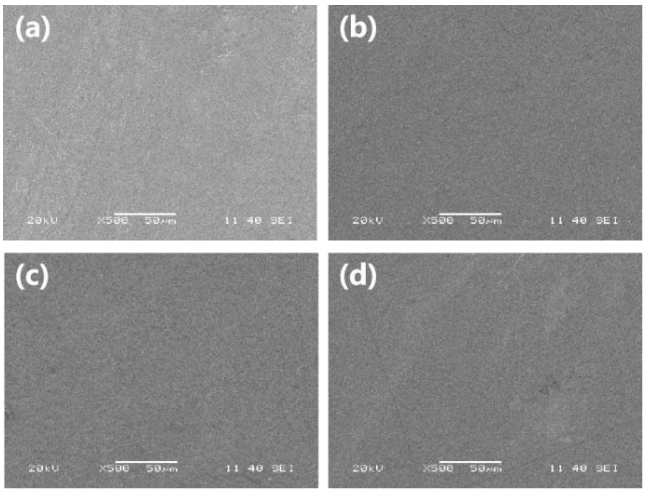


Fig.1 Surface SEM morphologies of $FeCrNiMoNb_x$ high-entropy alloy coatings prepared under different Nb target powers: (a) 15 W, (b) 25 W, (c) 50 W, (d) 75 W

Table 1 EDS composition table of $FeCrNiMoNb_x$ multi-component alloy coating under different Nb target power conditions (at.%)

Power	Fe	Cr	Ni	Mo	Nb	x
15W	23.13	24.22	19.82	24.13	8.70	0.3
25W	22.33	23.77	19.64	22.27	11.99	0.5
50W	18.76	19.44	16.48	21.47	23.85	1.2
75W	19.47	19.42	16.61	19.05	25.45	1.4

ISSN: 3007-9640 DOI: https://doi.org/10.70114/acmsr.2026.9.1.P172

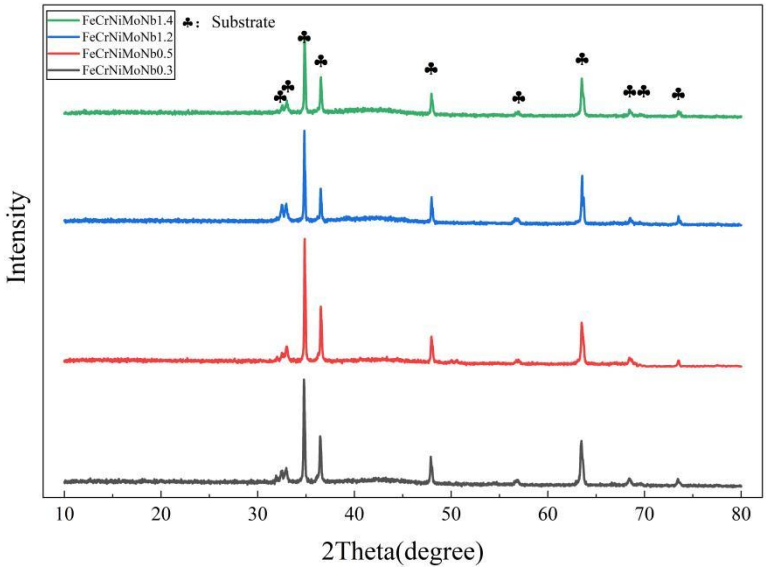


Fig. 2 XRD patterns of FeCrNiMoNb$_x$ (x = 0.3, 0.5, 1.2, 1.4) high-entropy coatings with different Nb contents

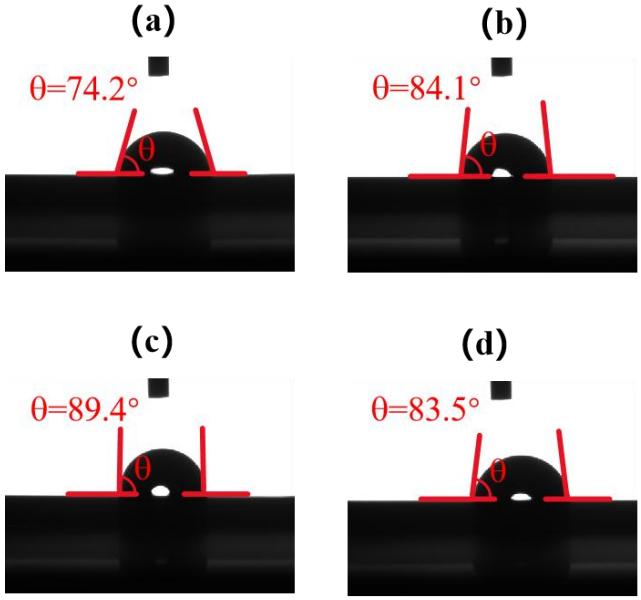


Fig. 3 Water contact angle images of FeCrNiMoNb$_x$ high-entropy alloy coatings with different Nb contents
(a) FeCrNiMoNb$_{0.3}$, (b) FeCrNiMoNb$_{0.5}$, (c) FeCrNiMoNb$_{1.2}$, (d) FeCrNiMoNb$_{1.4}$

3.2 Corrosion Behavior in NaCl solution

The potentiodynamic polarization curves of the Zr substrate and FeCrNiMoNb$_x$ coatings in 3.5 wt.% NaCl solution are shown in Fig. 4, and the corresponding electrochemical parameters are listed in Table 2. The corrosion current densities of the Zr substrate, FeCrNiMoNb$_{0.3}$, FeCrNiMoNb$_{0.5}$, FeCrNiMoNb$_{1.2}$, and FeCrNiMoNb$_{1.4}$ were 1.31×10^{-7}, 7.72×10^{-7}, 4.59×10^{-7}, 9.30×10^{-8}, and 8.50×10^{-8} A/cm^2, respectively. The FeCrNiMoNb$_{1.2}$ and FeCrNiMoNb$_{1.4}$ coatings showed lower corrosion current densities than the Zr substrate, indicating that higher Nb contents improved the corrosion resistance in Cl^--containing solution. This improvement may be related to the denser coating structure and the formation of more stable passive products containing Nb, Cr, and Mo.

ISSN: 3007-9640 DOI: https://doi.org/10.70114/acmsr.2026.9.1.P172

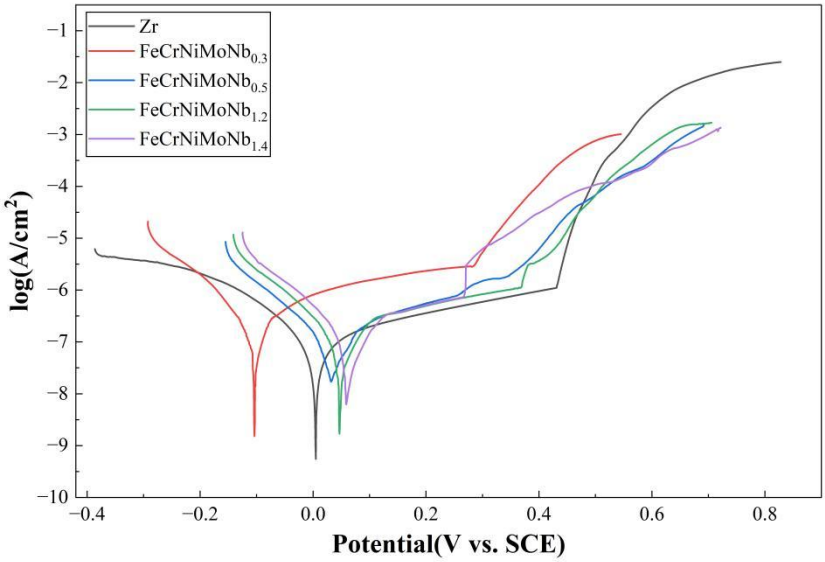


Fig. 4 Potentiodynamic polarization curves of $FeCrNiMoNb_x$ (x=0.3, 0.5, 1.2, 1.4) high-entropy alloy coatings with different Nb contents in 3.5 wt.% NaCl solution

Table 2 Electrochemical corrosion parameters of $FeCrNiMoNb_x$ (x=0.3, 0.5, 1.2, 1.4) high-entropy alloy coatings with different Nb contents

Alloys	Corrosion potential (V)	Corrosion current density (A/cm2)
Zr	0.0047	1.31×10-7
FeCrNiMoNb0.3	-0.1038	7.72×10-7
FeCrNiMoNb0.5	0.0318	4.59×10-7
FeCrNiMoNb1.2	0.0465	9.30×10⁻8
FeCrNiMoNb1.4	0.0589	8.50×10⁻8

3.3 Corrosion Behavior in High-Temperature and High-Pressure Water

The mass changes after high-temperature and high-pressure water corrosion are listed in Table 3. After corrosion at 360 °C and 18.6 MPa for 72 h, the $FeCrNiMoNb_{0.3}$, $FeCrNiMoNb_{0.5}$, $FeCrNiMoNb_{1.2}$, and $FeCrNiMoNb_{1.4}$ coatings showed mass changes of −64.92, −44.72, −5.69, and −9.38 mg/dm^2, respectively. The $FeCrNiMoNb_{1.2}$ coating exhibited the smallest mass loss. As shown in Fig. 5, the $FeCrNiMoNb_{1.2}$ coating retained better surface integrity after corrosion. Fig. 6 shows that the main corrosion products of $FeCrNiMoNb_{1.2}$ were Cr_2O_3, Nb_2O_5, and ZrO_2. The formation of Cr_2O_3 and Nb_2O_5 contributed to the protective oxide layer, which hindered the inward diffusion of corrosive species. In addition, the cross-sectional EDS line-scan results in Fig. 7 further confirmed the elemental distribution after corrosion. Therefore, $FeCrNiMoNb_{1.2}$ showed the best overall corrosion resistance among the investigated coatings.

Table 3 Average mass change per unit area of $FeCrNiMoNb_x$ (x = 0.3, 0.5, 1.2, 1.4) high-entropy alloy coatings with different Nb contents after high-temperature and high-pressure water corrosion

Alloys	Average weight gain per unit area (mg/dm^2)
Zr	33.33
$FeCrNiMoNb_{0.3}$	-64.92
$FeCrNiMoNb_{0.5}$	-44.72
$FeCrNiMoNb_{1.2}$	-5.69
$FeCrNiMoNb_{1.4}$	-9.38

ISSN: 3007-9640 DOI: https://doi.org/10.70114/acmsr.2026.9.1.P172

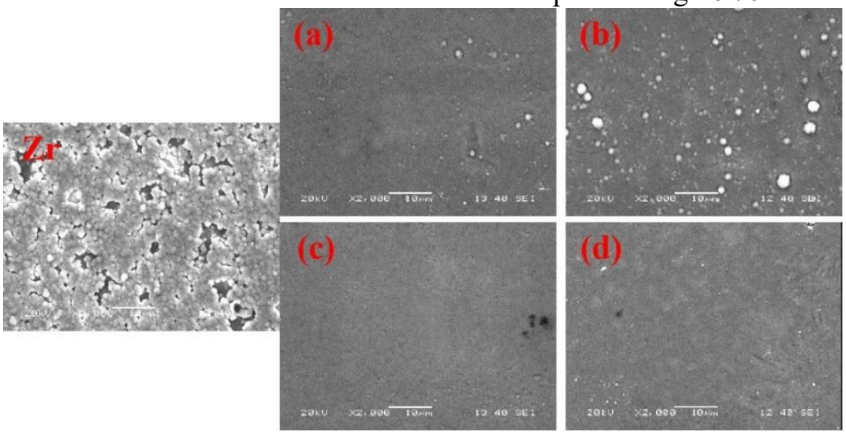


Fig. 5 Surface SEM morphologies of Zr substrate and FeCrNiMoNb$_x$ high-entropy alloy coatings with different Nb contents after high-temperature and high-pressure water corrosion
(a) FeCrNiMoNb$_{0.3}$, (b) FeCrNiMoNb$_{0.5}$, (c) FeCrNiMoNb$_{1.2}$, (d) FeCrNiMoNb$_{1.4}$

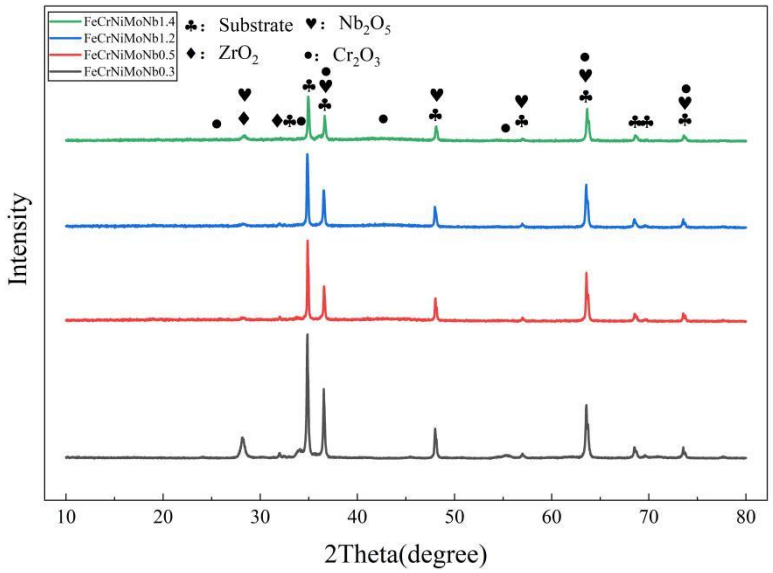


Fig. 6 XRD patterns of FeCrNiMoNb$_x$ (x = 0.3, 0.5, 1.2, 1.4) high-entropy alloy coatings with different Nb contents after high-temperature and high-pressure water corrosion

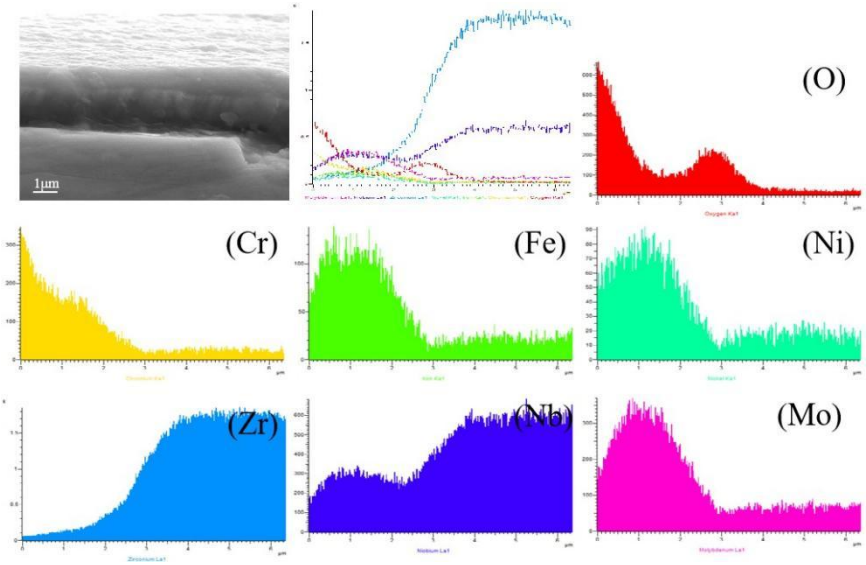


Fig. 7 Cross-sectional EDS line-scan results of FeCrNiMoNb$_{1.2}$ high-entropy alloy coating after high-temperature and high-pressure water corrosion

ISSN: 3007-9640 DOI: https://doi.org/10.70114/acmsr.2026.9.1.P172

Summary

$FeCrNiMoNb_x$ HEA coatings with different Nb contents were successfully prepared on Zr alloy substrates by magnetron co-sputtering. All coatings were continuous and mainly exhibited amorphous or low-crystallinity structures. Among them, the $FeCrNiMoNb_{1.2}$ coating showed the smoothest and densest surface, the largest water contact angle of 89.4°, and the best integrity after high-temperature and high-pressure water corrosion. In 3.5 wt.% NaCl solution, $FeCrNiMoNb_{1.2}$ and $FeCrNiMoNb_{1.4}$ exhibited lower corrosion current densities than the Zr substrate. Overall, $FeCrNiMoNb_{1.2}$ showed the best comprehensive protective performance and is a promising candidate coating for ATF cladding applications.

Acknowledgements

The present work was financially supported by Postgraduate Research & Practice Innovation Program of Jiangsu Province [Grant No. KYCX25_4343].

References

[1] Ungar T, Ribarik G, Topping M, et al. Characterizing dislocation loops in irradiated polycrystalline Zr alloys by X-ray line profile analysis of powder diffraction patterns with satellites[J]. Journal of Applied Crystallography, 2021, 54: 803-821.

[2] Lei P, Ran G, Liu C, et al. In Situ TEM Study of Microstructure Evolution of Zr-Nb-Fe Alloy Irradiated by 800 keV Kr2+ Ions[J]. Materials, 2017, 10(4): 437.

[3] Li F, Li S, Tong H, et al. The Application of Chemical Polishing in TEM Sample Preparation of Zirconium Alloys[J]. Materials, 2020, 13(5): 1036.

[4] Tang Y-Y, Chang Y-L, Luo W, et al. High-Temperature Oxidation Behavior of TiN-, Cr-, and TiN-Cr PVD-Coated Zircaloy 4 Alloy at 1200 °C[J]. Materials, 2025, 18(8): 1692.

[5] Li Y, You E, Wang T, et al. Developments, challenges and prospects in thermal-hydraulic research on accident tolerant fuel[J]. Heliyon, 2024, 10(19).

[6] Li K, Trofimov V, Han C, et al. The Printability, Microstructure, and Mechanical Properties of Fe80-xMnxCo10Cr10 High-Entropy Alloys Fabricated by Laser Powder Bed Fusion Additive Manufacturing[J]. Micromachines, 2024, 15(1): 123.

[7] Zhang D, Wu Q, Wu L, et al. Optimal Electrocatalyst Design Strategies for Acidic Oxygen Evolution[J]. Advanced Science, 2024, 11(38): 2401975.

[8] Badea T A, Condruz M R. Investigation on Improving the Hot Corrosion Resistance of Selective Laser Melting Manufactured Inconel 625 by Pre-Oxidation Heat Treatment[J]. Materials, 2025, 18(5): 1111.

[9] Ndumia J N, Kang M, Gbenontin B V, et al. A Review on the Wear, Corrosion and High-Temperature Resistant Properties of Wire Arc-Sprayed Fe-Based Coatings[J]. Nanomaterials, 2021, 11(10): 2527.

[10] Liao J, Zhang L, Peng C, et al. Fabrication of Ni-Cu-W Graded Coatings by Plasma Spray Deposition and Laser Remelting[J]. Materials, 2022, 15(8): 2911.

[11] Zhao Y, Wu J, Cao X, et al. High-Entropy Materials for Water Splitting: An Atomic Nanoengineering Approach to Sustainable Hydrogen Production[J]. Advanced Materials, 2025, 37(36): 2506117.

[12] Novak P, Bellezze T, Cabibbo M, et al. Solutions of Critical Raw Materials Issues Regarding Iron-Based Alloys[J]. Materials, 2021, 14(4): 899.

[13] Liu H, Huang L, Liu S, et al. Evolution of temporomandibular joint reconstruction: from autologous tissue transplantation to alloplastic joint replacement[J]. International Journal of Oral Science, 2025, 17(1): 17.

[14] [14] Zeng Z, Gu S, Wang J, et al. Passivation performance of Nb microalloyed rebar in concrete carbonation environments with different pH[J]. Scientific Reports, 2024, 14(1): 22919.